Comparison between the Seismic Performance of Buried Pipes and Pipes in a Utility Tunnel

Wei Liu[1, 2, *] and Qianxiang Wu[2]

Abstract: A utility tunnel system consists of pipes and ancillary facilities. In this paper, a finite element model of a concrete utility tunnel with pipes inside is established. Several tunnel segments were built to simulate a real utility tunnel, while the pipe was fixed by springs on the brackets in the utility tunnel. Using the discrete soil spring element to simulate the soil-structure interaction, actual earthquake records were adopted as excitation to analyze the seismic responses of pipes in a utility tunnel. Moreover, the influences of different parameters, including soil type, earthquake records, and field apparent wave velocity on the seismic responses of the utility tunnel and the pipes inside were studied. Finally, the seismic responses of buried pipes were analyzed and compared with those of pipes in a utility tunnel to evaluate the seismic performance of pipes for two working conditions.

Keywords: Pipe in utility tunnel, buried pipe, seismic performance.

1 Introduction

Lifeline engineering systems refer to engineering facilities that maintain the functions of modern cities and regional economy [Li (1999)]. As important components of urban lifeline systems, buried pipe networks play a crucial role in modern cities. Pipes are subject to many external influences during use that cause damage, such as upper loading, traffic loads [Li, Fang, He et al. (2019)], and internal pressure [Hu, Fang, Wang et al. (2019)]. In addition, the excavation, unloading, and other processes during the construction process cause changes in the ground stress [Su, Kang, Wang et al. (2016); Li, Fang, He et al. (2017); Wu, Xiang, Chen et al. (2019)], which may also cause damage to the pipes. In addition to these conventional factors, pipes may be affected by a variety of disasters such as earthquakes, landslides [Mandolini, Minutolo and Ruocco (2001)], and mining [Cao, Zhou, Xu et al. (2014)]. The impact of landslides and mining is mostly limited to long-distance pipelines in wild areas, and earthquakes can easily

[1] State Key Laboratory of Disaster Reduction in Civil Engineering, Tongji University, Shanghai, 200092, China.
[2] Department of Structural Engineering, Tongji University, Shanghai, 200092, China.
* Corresponding Author: Wei Liu. Email: liuw@tongji.edu.cn.
Received: 25 June 2019; Accepted: 16 January 2020.

affect urban pipe networks, which can lead to malfunctions in a city, or even secondary disasters. For example, after the Wenchuan earthquake (M_L=8.0) in 2008, gas supply facilities in the disaster area suffered serious damage. In Deyang, over 100 breaks appeared on the transportation and distribution gas pipes, and more than 20 valve wells were damaged [Wang, Guo and Zhang (2012)]. The water supply facilities also suffered massive damage. In Dujiangyan, more than 2,000 breaks appeared on 380 km of water pipes. As a result, the leakage rate of the water distribution network was up to 65% [State Key Laboratory of Disaster Reduction in Civil Engineering (2008)].

Recently, utility tunnels have been developing rapidly, especially in China. A utility tunnel refers to a modern and intensive urban lifeline infrastructure formed by centrally arranging two or more urban pipes in the same artificial space. The earliest exploration and construction of a utility tunnel began in 1833 in Paris, France. Since 2006, many cities in China, such as Shanghai, Guangzhou, Ningbo, and Shenzhen, have begun the construction of utility tunnels. A tunnel will also suffer damage during an earthquake [Lai, He, Qiu et al. (2017)], so it is necessary to consider the aseismic problem of a utility tunnel. Because utility tunnels are similar to traditional tunnels, seismic analysis should include analytical methods, common displacement, reaction displacement, and numerical methods. For the analytical methods, the tunnel is regarded as a hole in infinite or semi-infinite media space, and a wave equation is solved in order to determine the seismic responses. Pao et al. [Pao (1962); Chao (1973)] used the wave function expansion method to solve the problem of a circular cavity in an infinite space subjected to a P wave. Given the fact that an actual tunnel is in a semi-infinite space, Lee [Lee (1979)] studied the seismic responses of a tunnel subjected to an SH wave in elastic half-space. Additionally, Luco et al. [Luco and de Barros (1994)] studied the seismic responses under an SV wave. However, due to the complexity of a site in actual engineering, the application of an analytical solution is limited. The common displacement method is a method based on the theory of elastic wave propagation that considers whether the tunnel strain is equal to the field strain. In other words, the method ignores the slippage between tunnels and the surrounding soil. Using this method, Kuesel et al. [Kuesel (1969); St John and Zahrah (1987)] provided the maximum strains of tunnels under P, S, and Rayleigh waves. Although this method ignores the interaction between the soil and the structures, the essential problem is that the field strain determines the structural strain and then directs the subsequent work. Unlike the common displacement method, the reaction displacement method considers the slippage between tunnels and the surrounding soil, which is viewed as both springs and damping, in order to determine the seismic response of tunnels. The focus of the method is finding the equivalent damping coefficient and the spring stiffness of soil. Bettess et al. [Bettess and Zienkiewica (1977)] used semi-infinite plane elastic foundations to simulate the spring stiffness. Subsequently, Song et al. [Song and Wolf (1994, 2000)] proposed a method to obtain the damping. With the development of computer technology, numerical methods such as the finite element [Li, Fang, He et al. (2017); Wu, Xiang, Chen et al. (2019)], boundary element, discrete element, and finite difference methods [Zhao and Song

(2015)] have become important tools for analyzing the seismic responses of tunnels. For buried pipes, the analytical [Parmelee and Ludtke (1975)], common displacement [Newmark (1967)], response displacement [Kuribayashi, Iwasaki and Kawashima (1974); Shinozuka and Koike (1979); Wang and Cheng (1979)], and numerical methods [Bao, Xia, Ye et al. (2017); Liu, Sun, Miao et al. (2015); Sun (2012); Kuwata, Takada and Yamasaki (2008)] are also available for obtaining the seismic responses. In addition, tunnels have been tested on shaking tables [Xu, Li, Xia et al. (2016); Yu, Yan, Bobet et al. (2017); Yu, Yuan, Xu et al. (2018a)].

Some studies about utility tunnels subjected to earthquakes have been reported. In 2010, Chen et al. [Chen, Shi and Li (2010)] used an inter-layer shearing box to conduct a shaking table test for a utility tunnel with and without joints. Additionally, Jiang et al. [Jiang, Chen and Li (2009)] performed a numerical simulation of utility tunnels. However, these studies did not consider pipes in utility tunnels. In 2012, Tang et al. [Tang, Gai, Wen et al. (2012)] conducted shaking table tests and numerical simulations on utility tunnels with pipes inside. However, their work mainly focused on the weakening effect of the vibration-isolating device on the acceleration of the pipe in the utility tunnel, and the seismic responses of the pipe were not analyzed. Although some scholars have studied the seismic performance of utility tunnels, research on the seismic performance of the pipes inside is lacking. In this paper, the seismic responses of pipes in utility tunnels are analyzed and compared with those of buried pipes. This paper is organized as follows. Following the introduction, the second section introduces the method for modeling the utility tunnel. Springs were adopted to describe the interactions between the structures and the soil, and the seismic displacement time history was utilized to consider the traveling wave effect. The third section analyzes the seismic responses of the pipes in an actual utility tunnel. The influences of different parameters, including site type, wave apparent velocity, and earthquake records, were investigated. The fourth section introduces the method for analyzing the seismic responses of buried pipes. The responses are compared with those of the pipes in utility tunnels. The fifth section gives the conclusions.

2 Modeling for utility tunnel system

2.1 Model details

A utility tunnel system is usually composed of an outer tunnel and internal pipes. The outer tunnel is usually a square or rectangular reinforced concrete lining. To separate gas and sewage pipes from other pipes, a tunnel is usually separated into several rooms. In the longitudinal direction, a tunnel is connected by several segments via joints. Generally, there is no structural connection at the joints. Thus, the steel bars and the concrete are discontinuous at the joints, and only waterproof treatment is implemented. Therefore, the mechanical relationship of the two segments of a utility tunnel only involves collision. In China, the maximal length of each segment is 30 m for the convenience of construction. Inside a tunnel, pipes are fixed on support piers or brackets.

For the seismic analysis of buried structures, many researchers [Liu, Sun, Miao et al. (2015); Sun (2012); Yue (2007); Wang and Cheng (1979)] have indicated that the inertial effect is small, and the quasi-static response accounts for the majority of the effect. Thus, the quasi-static method was employed in this research. Given that the utility tunnel was a long-line structure, a ground motion field model had to be considered. For simplification, the traveling wave effect was considered in order to establish the ground motion field model. Moreover, the soil-structure interaction could be simulated by the axial and lateral springs. One end of the springs connected with the structures, while the ground motion was input from another end.

In this study, ABAQUS software, a widely adopted finite element software, was employed to obtain the seismic responses of tunnels and pipes. For tunnel structures, which are reinforced concrete structures, a mature model was available. A solid element (C3D8R) was chosen for the concrete, and a truss element (T3D2) was chosen for the steel bars. Steel bars were embedded into the concrete entities to make them work together, and the contact between the concrete and the steel bars was neglected; i.e., there was no slippage between the steel bars and the concrete. The ideal elastoplastic models were adopted to describe the stress and strain relationships of the steel bar and the concrete, which are shown in Figs. 1 and 2. In the figures, f_y is the yield strength of the steel bar, and ε_y is the corresponding strain at the time of yielding. f_c and f_t are the compressive strength and the tensile yield strength of concrete, respectively, and ε_c and ε_t are the corresponding strains. A C3D8R element was chosen for the pipes. All the element sizes were about 0.4 m. The pipes were fixed on the piers but they could move freely along the axial direction. To fix the pipe on the piers, two springs were arranged on each pier to simulate

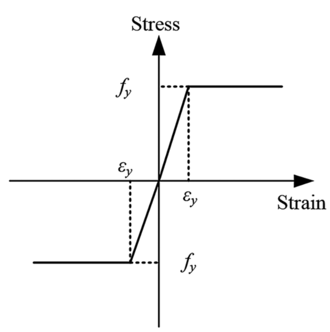

Figure 1: Stress-strain curve of the steel pipe and the steel bar

pipe clamps. In the actual engineering, the connection was constructed in the form of a copper and rubber waterproof joint that could bear compression but not any tension. To describe the collision between two segments, a connector element was used for the simulation of a joint. The relationship between the joint deformation and the spring stiffness is shown in Fig. 3. The origin of the joint deformation represented the initial position of the two segments of the utility tunnel. When the joint deformation was just

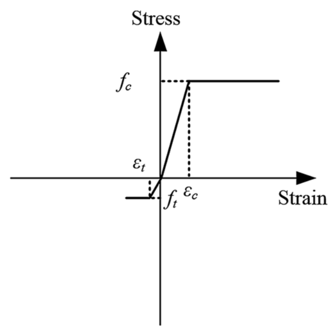

Figure 2: Stress-strain curve of the concrete

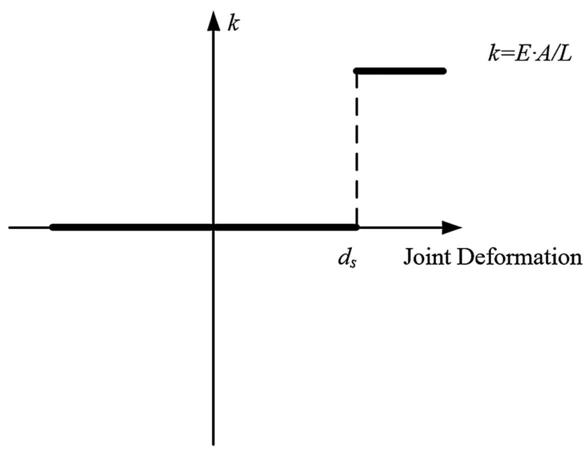

Figure 3: Spring stiffness and joint deformation between two segments of the utility tunnels

d_s, i.e., the space between two segments, then two utility tunnels had contact with each other. Moreover, when the joint deformation continued to increase, two utility tunnels collided, and the stiffness increased from zero to k=EA/L, where E is the elastic modulus of the tunnel, A is the section area, and L is the length of the segment.

Connector elements were used to describe the axial and transverse springs. The springs could be realized using Cartesian and Cardan connectors. This connector unit is a beam unit that can define stiffness in three directions and reflect the spring stiffness in three directions. To describe the continuity of the soil, the spring units needed to be dense enough. A space of two meters was adopted. In addition, the spring stiffness was derived based on the ALA-ASCE guidelines [American Lifeline Alliance (2001, 2005)]. The guidelines consider various variables such as soil quality, pipe diameter, and buried depth, and give the spring stiffnesses in the axial, transverse horizontal, and transverse vertical directions. The force-displacement relationships of the springs in three directions are shown in Fig. 4. Fig. 4(a) denotes the axial load-deformation relationships, Fig. 4(b)

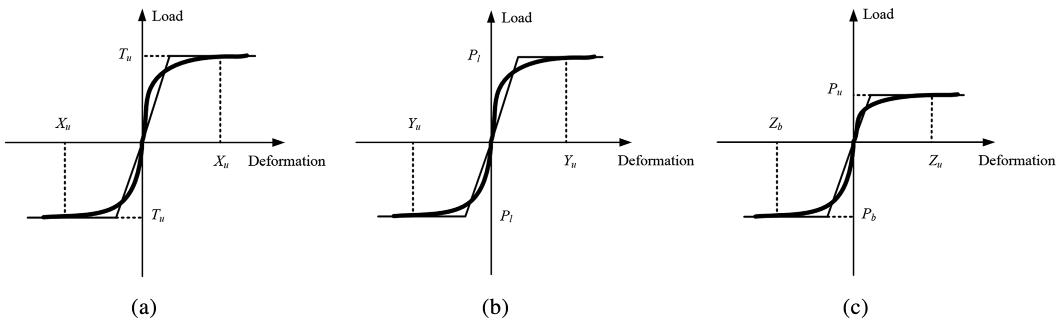

Figure 4: Load-deformation relationships for the soil-springs. (a) Axial spring. (b) Transverse horizontal spring. (c) Transverse vertical spring

denotes the transverse horizontal load-deformation relationships, and Fig. 4(c) denotes the relationship in the transverse vertical direction. T_u and P_l represent the maximal soil resistance before the soil-structure relationship failed, while X_u and Y_u represent the maximal deformation when the maximal soil resistance was developed in the axial direction and the transverse horizontal direction, respectively. The maximal soil resistances in the two vertical directions were different; specifically, the downward resistance was much greater than the upward resistance.

In Fig. 4, the nonlinear relationship between the force and the deformation of the soil spring (shown by the thick solid line) was simplified by an ideal elastoplastic model. The equivalent spring stiffness could be determined by the following formula [O'Rourke and Liu (1999)]:

$$K = \frac{2F}{\Delta} \tag{1}$$

where $F = T_u, P_l, P_u, P_b$ and $\Delta = X_u, Y_u, Z_u, Z_b$.

2.2 Earthquake input

Different from aboveground structures, the stiffness and natural frequency of underground structures are much higher caused by its interaction with surrounding soil. For example, the first natural frequency of buried pipes is usually larger than 100 Hz [Qu and Wang (1993)]. When the low-frequency earthquake wave acts as a dynamic excitation, the dynamic response of underground structures is unobvious and almost equal to the static one. This conclusion has been verified by some researches [Qu and Wang (1993), Liu and Li (2008), Sun (2012)]. Therefore, it is reasonable and efficient to analyze the seismic response of underground structures by the quasi-static method [Yu, Zhang, Chen et al. (2018b); Liu, Sun, Miao et al. (2015)]. This method was first proposed by Wang et al. [Wang and Cheng (1979)], which has been widely used. In this method, the scattering and reflection effects of seismic wave can be ignored. So, only the traveling wave effect is considered in this paper.

In the process of seismic wave propagation, the motion law of particles in soil obeys the general wave equation as shown in Eq. (2) [Liao (2002)].

$$\frac{\partial^2 u}{\partial t^2} = v^2 \frac{\partial^2 u}{\partial x^2} \tag{2}$$

where u is the amplitude of particle, x is the position parameter of particle, t is the time parameter of particle and v is field apparent wave velocity.

To solve the above equation, the following variable substitution as Eq. (3) is adopted.

$$\begin{cases} \xi = x - vt \\ \eta = x + vt \end{cases} \tag{3}$$

Then, Eq. (4) can be derived from the chain rule.

$$\begin{cases} \dfrac{\partial^2 u}{\partial x^2} = \dfrac{\partial^2 u}{\partial \xi^2} + 2\dfrac{\partial^2 u}{\partial \xi \partial \eta} + \dfrac{\partial^2 u}{\partial \eta^2} \\ \dfrac{\partial^2 u}{\partial x^2} = c^2 \left(\dfrac{\partial^2 u}{\partial \xi^2} + 2\dfrac{\partial^2 u}{\partial \xi \partial \eta} + \dfrac{\partial^2 u}{\partial \eta^2} \right) \end{cases} \tag{4}$$

After substituting Eq. (4) into Eq. (2), the following equation is derived:

$$\frac{\partial^2 u}{\partial \xi \partial \eta} = 0 \tag{5}$$

After integrating Eq. (5), it can give:

$$u(x,t) = f(x - vt) + g(x + vt) \tag{6}$$

where f and g are functions for describing the vibration form of soil particles, the independent variables of the function reflect the propagation characteristics of the wave. In one-dimensional case, they represent the forward and backward waves respectively. It is worth noting that there are only two propagation directions for the origin. For the other points, there is actually only one propagation direction, that is, the forward propagation of the wave. The physical meaning of the independent variable x-vt is explained later.

It is assumed that the motion of the particle in the soil at a fixed point $x = x_1$ is as shown in Eq. (7).

$$u(x_1, t) = f(x_1 - vt) \tag{7}$$

Then at another fixed point $x = x_2 (x_2 > x_1)$, the motion of the particle can be written as:

$$u(x_2, t) = f(x_2 - vt) = f\left[x_1 - v\left(t - \frac{x_2 - x_1}{v}\right)\right] \tag{8}$$

Eq. (8) shows that at x_1, x_2, except for the time lag of $(x_2 - x_1)/v$, which is the time of wave propagation at this distance, the wave shapes of them are the same.

Eq. (7) also can be written as:

$$u(x,t) = f\left(t - \frac{x}{v}\right) \tag{9}$$

Then, when the ground motion displacement at the first point is known as $u(x_0, t)$, the displacement at point x_i, $u(x_i, t)$, is:

$$u(x_i, t) = u\left(t - \frac{x_i - x_0}{v}\right), \tag{10}$$

where v is the field apparent wave velocity of the seismic wave along the axial direction of the structures, which can be written as:

$$v = \frac{v_s}{\sin\theta}, \tag{11}$$

where v_s is the propagation velocity of the seismic wave, and θ is the angle between the direction of seismic wave propagation and the axial direction of the structures. It is worth noting that, since the length of the model established later is not large, it is considered reasonable that not to consider the wave attenuation in the process of wave propagation.

To enable the model to reflect the effects of the ground motion in different directions simultaneously, an obliquely incident seismic wave input was applied. The incident direction of the waves is shown in Fig. 5. The angles between the seismic propagation direction and the x, y, and z axes are all 60°. The incident direction is simply the direction that had the same angle between the three coordinate axes. Therefore, the seismic waves could be decomposed into three identical waves along the x, y, and z axes.

Since the dimensions of utility tunnel and pipe model in z direction are much larger than those in x and y direction, it can be considered that $u(x,t)$ of all points on each cross section is the same, and $u(x_i, t)$ at any cross section can be calculated according to Eqs. (10) and (11).

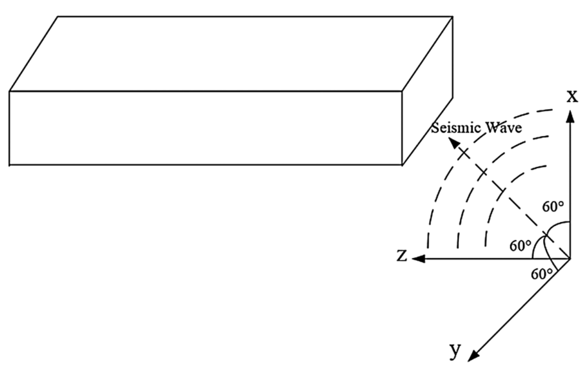

Figure 5: The incident angle of the seismic wave

Assuming that the ground motion displacement at the starting point of the model is $u(x_0, t)$, the ground motion displacement $u(x_i, t)$ can be expressed as Eq. (12) for all points on the cross section at $x = x_i$.

$$u(x_i, t) = u\left(t - \frac{x_i - x_0}{v_s/\sin\theta}\right), \tag{12}$$

where $u(x_0, t)$ is the earthquake displacement records, v_s is determined by sites and $\theta = 60°$ in this paper. These variables are expressed in Fig. 6. The earthquake displacement history lasted for 20 s, while the time step was 0.01 s. A 20 s duration was adopted because it is long enough to cover the entire strong earthquake stage and give the maximum displacement response of the structure.

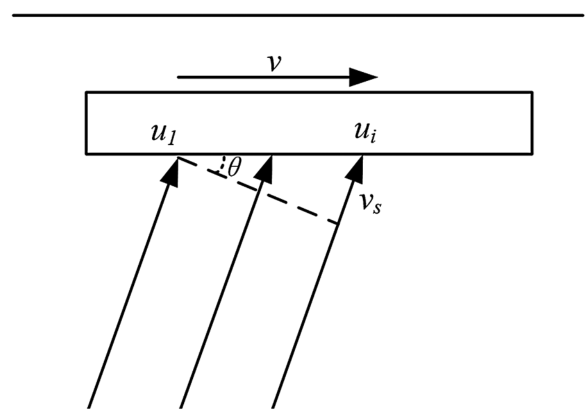

Figure 6: Traveling-wave effect

3 Numerical result and analysis

3.1 Case study

To obtain the seismic responses of pipes in a utility tunnel, an FEM model was established based on a double cabin utility tunnel project in Chengdu with two continuous steel pipes inside. According to the Chinese Code [Ministry of Housing and Urban-Rural Development of the China (2015)], four sites, Sites I to IV, were considered. The parameters for each site are given in Tab. 1. Two corresponding actual earthquake records, shown in Tab. 2, were selected for analysis. It is worth noting that these four types of sites corresponded to gravel, coarse sand, clay, and soft clay. The specific parameter values were selected according to actual engineering experience.

As shown in Fig. 7, the utility tunnel had two rooms to accommodate a DN400 pipe (with an external diameter of 426 mm and a wall thickness of 10 mm) and a D159 pipe (with an external diameter of 159 mm and a wall thickness of 6 mm). The pipes were fixed on concrete piers at a distance of 6 m. For convenient construction, the utility tunnel was

Table 1: Site parameters

Soil type	I	II	III	IV
Internal friction angle (°)	50	40	30	20
Cohesive force (kPa)	0	0	4	8

Table 2: Earthquake records for different sites

Site	Records
I	1985, La Union, Michoacan Mexico
	1994, Los Angeles Griddith Observation
II	1952, Taft Lincoln school tunnel, California
	1979, El Centro, Array#10, Imperial valley
III	1984, Coyote Lake Dam, Morgan Hill
	1940, El Centro- Imp Vall Irr Dist, El Centro
IV	1981, Westmorland, Westmorland
	1976, Tianjin Hospital, Tangshan

Table 3: Spring stiffness

Site	I	II	III	IV
Axial (kN/m^{-2})	8.52×10^8	5.22×10^8	2.85×10^8	6.3×10^7
Transverse (horizontal) (kN/m^{-2})	4.78×10^7	2.64×10^7	1.17×10^7	5.35×10^6
Transverse (vertical downwards) (kN/m^{-2})	2.96×10^8	6.98×10^7	2.79×10^7	1.42×10^7
Transverse (vertical upwards) (kN/m^{-2})	1.11×10^8	4.85×10^7	2.56×10^7	1.95×10^7

composed of segments with lengths of 25 m. The joints between two segments were waterproofed construction that could not bear any load. The reinforcement drawing of the utility tunnel is shown in Fig. 8, and a reinforcement bar lofting drawing of the utility tunnel is shown in Fig. 9.

In reality, the utility tunnels were very long, even longer than 10 km. However, a very long model was not needed because the computation cost would be very high if the model was too long. The length of the model depended on whether the boundary conditions influenced the seismic response of the middle part of the utility tunnel. Moreover, 100 m and 150 m long utility tunnels were previously tried, and it was found that the maximum stress of the pipe was essentially the same as that of a 75 m tunnel. In this research, a 75 m long

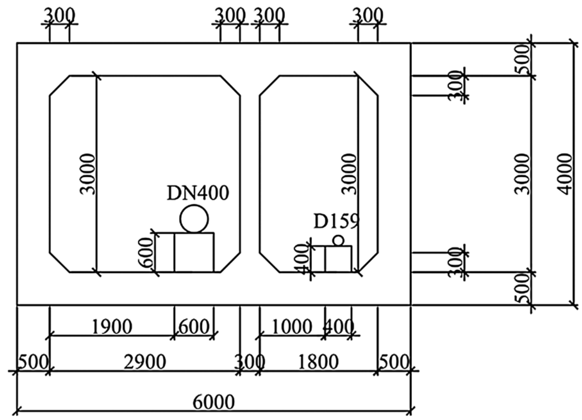

Figure 7: Cross section of the utility tunnel

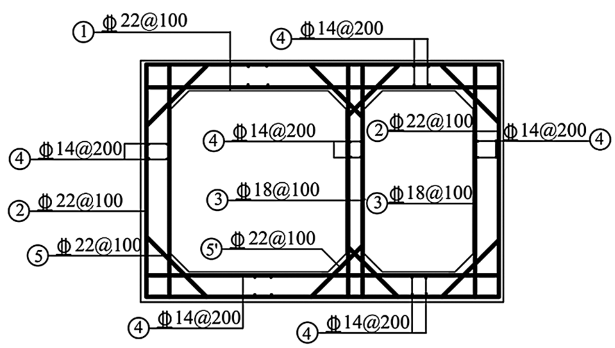

Figure 8: Reinforcement drawing of the utility tunnel

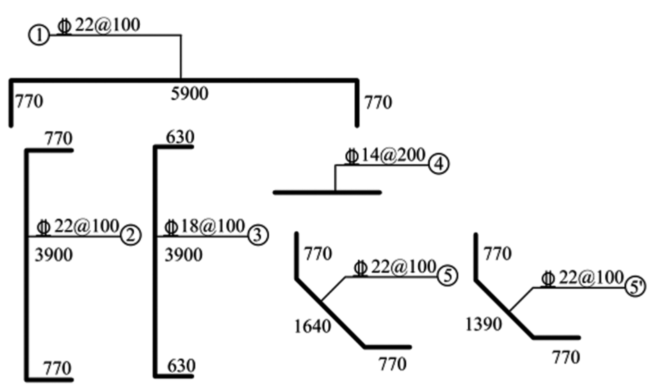

Figure 9: Steel lofting drawing of the utility tunnel

utility tunnel system, i.e., three segments, was enough to avoid the influence of boundary conditions. In addition, in order to simulate the long pipe in the utility tunnel, a bending spring was applied to both ends of the pipe in the model, and the spring stiffness was calculated from the bending modulus of the pipe. Considering the way that the pipe piers were connected to the pipe in the utility tunnel, the axial deformation was not constrained at the end of the pipe.

Soil spring units were arranged at a distance of 2 m in the axial direction of the utility tunnel. Along the outside surface of the cross section, the springs were spaced 2 m apart, and the distance from the corner was 1 m. In the axial direction, there were 36 groups of soil springs. Each group consisted of three soil springs in both the bottom and the top surfaces and two in each side surface. Therefore, there were 360 spring units surrounding the utility tunnel. The schematic of the model is shown in Fig. 10. The layout of the soil springs is shown in Fig. 11(a), while a single soil spring is illustrated in Fig. 11(b). The pipes in the utility tunnel are shown in Fig. 11(c). Finally, the entire utility tunnel is shown in Fig. 11(d). There were 91,446 nodes and 140,635 elements in this model. The damping coefficient was 0 in this model.

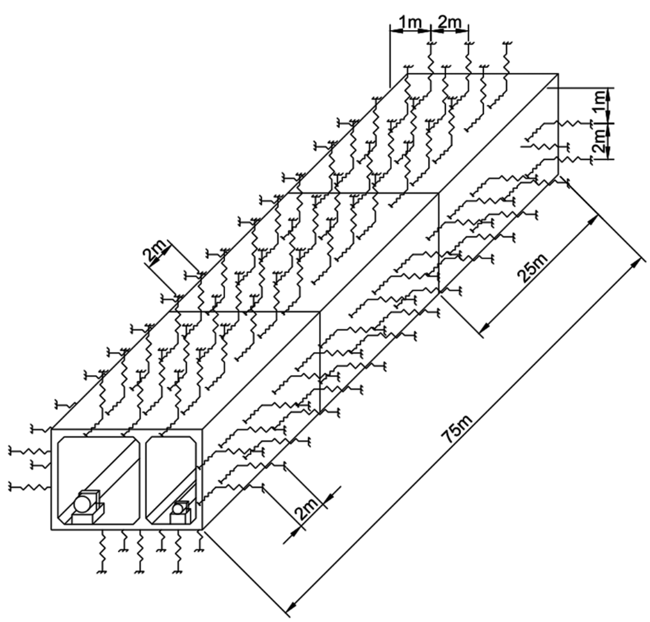

Figure 10: Schematic diagram of the utility tunnel model

3.2 Responses of utility tunnel under earthquakes

Firstly, the widely adopted El Centro wave was considered as the excitation. The apparent wave velocity was 1000 m/s, and the peak acceleration was adjusted to 0.2 *g* considering the earthquake intensity of VIII in the Chinese Code [Ministry of Housing and Urban-Rural

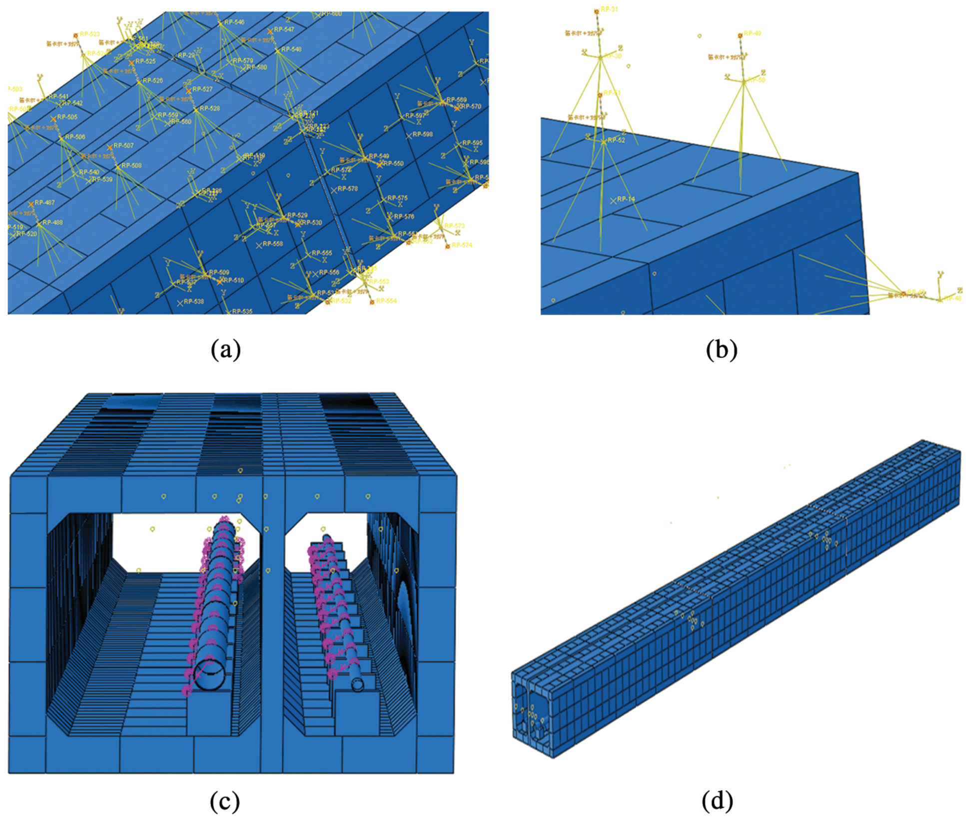

Figure 11: Model of utility tunnel. (a) Utility tunnel joints and soil spring. (b) Soil spring. (c) Pipes in the utility tunnel. (d) Entire utility tunnel

Development of the China (2015)]. All the seismic records lasted for 20 s. The seismic responses of the utility tunnel in site II were obtained. Fig. 12 shows the von-Mises stress contour of the concrete section at 7.0 s under the El Centro wave. Fig. 13 shows the von-Mises contour of the steel bars.

Fig. 14 shows a von-Mises contour of the pipe in the utility tunnel at 7.0 s. For convenience, we defined the largest stress at a point during the whole process as the maximal stress. Additionally, the largest value of the maximal stresses of all points was called the largest maximal stress. Only the pipe in the middle segment is shown in the figure, where the joints of the two utility tunnels are close to the Nos. 1 and 5 piers. Under the earthquake condition, the maximal stresses of the pipe occurred at the two piers closest to the joints of the utility tunnel, which were the largest and the second largest maximal stresses, i.e., 17.12 MPa and 16.97 MPa, respectively. Given that there was no structural connection at the joint between the two segments of the utility tunnel, a large deformation would appear at the joint. Given that the pipe was continuous, a large strain would appear at the

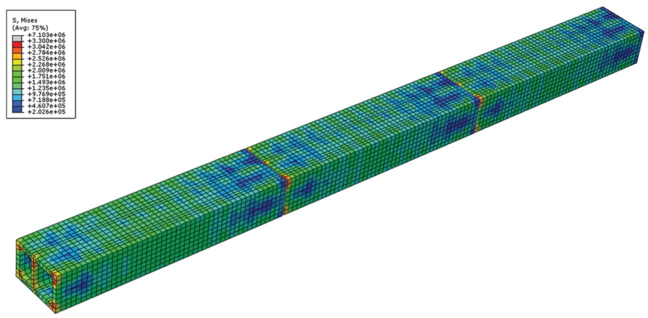

Figure 12: Von-Mises contour of the utility tunnel’s concrete section at 7.0 s

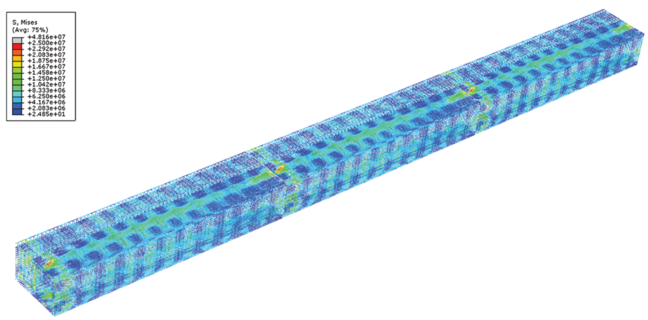

Figure 13: Von-Mises contour of the utility tunnel’s steel bars at 7.0 s

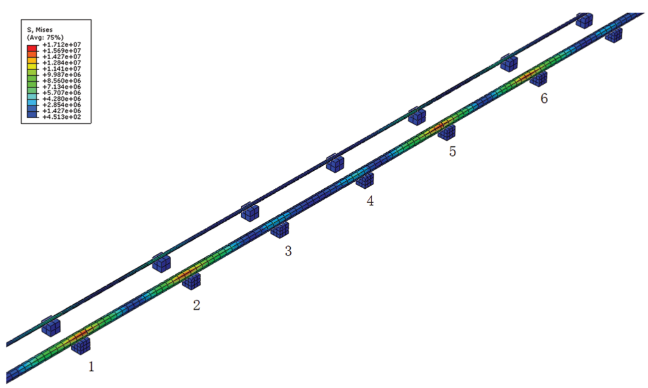

Figure 14:: Von-Mises contour of the pipes in the utility tunnel at 7.0 s

location of the joint, resulting in the large maximal stress. The stress around the joint was mainly caused by the bending stress. A detailed description of this is given in Section 4.3. Moreover, the pipe stress at the pier was larger than that of the suspended pipe. For example, the maximal stress at the No. 3 pipe pier was 5.37 MPa, and the maximal stress at the No. 4 pipe pier was 5.26 MPa, while the maximal stress of the suspended pipe was 0.82 MPa. For the pipes in the utility tunnels, the axial stress could be neglected because of the boundary conditions. However, due to the presence of the clamp, the movement of the pipe in the vertical direction was restricted. Thus, a larger bending moment was generated at the clamp, resulting in larger bending stress and larger von-Mises stress. Fig. 15 shows the Von-Mises stress envelope diagram of the pipes in the utility tunnel, wherein the distance refers to the distance from the end of the pipe where the seismic wave was input, along the direction of the pipe. Two double-peak protrusions on both sides appeared on the two piers at the joint of the two tunnels (Nos. 1, 2, 5, and 6 pipe piers), where the maximal stress occurred. For the middle part of the two protrusions, that is, the second section of the tunnel, it can be seen that the stress state of the pipe in the second section of tunnel tended to be stable. The minimal value appeared at 40 m (the middle of the Nos. 3 and 4 pipe piers) because there was a part of the suspended pipe, without the constraint of the pier and away from the joint, so the stress was small.

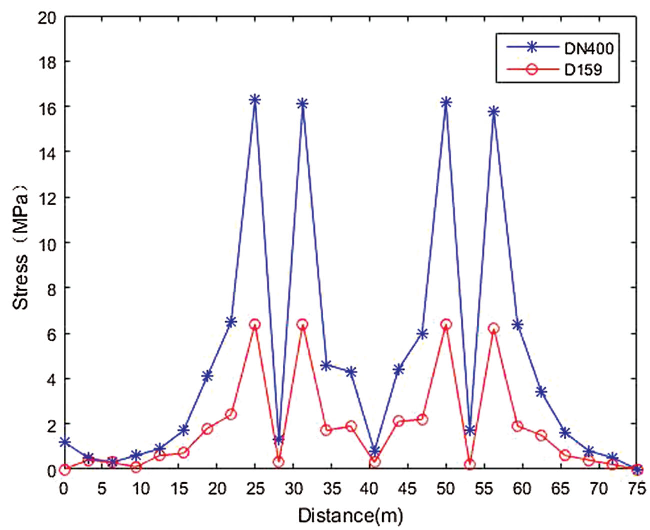

Figure 15: Von-Mises stress envelope diagram of the pipes in the utility tunnel

3.3 Influence of the site type

To study the influence of the site type, four sites were used to study the seismic responses according to the Chinese Code [Ministry of Housing and Urban-Rural Development of the China (2015)]. Sites I, II, III, and IV approximately corresponded to sites B, C, D, and E in the ASCE Guidelines [Sei, ASCE (2010)]. The specific parameters of these four sites are shown in Tab. 1. According to the ALA-ASCE guidelines [American Lifeline Alliance (2001, 2005)], which only covers circular pipes, the soil spring stiffness of four sites could be obtained, as shown in Tab. 3. For the utility tunnel, the principle of equal area was used to treat the utility tunnel as a circle to give the spring stiffness. For example, if the cross section of the utility tunnels was (4×6) m and its area was 24 m^2, then it was equivalent to a circle with diameter of 5.530 m, and its cross section area was 24 m^2.

The El Centro earthquake record in 1979 was chosen as the excitation, and the peak acceleration was adjusted to 0.2 *g*, which corresponded to the peak acceleration of the earthquake intensity of VIII in the Chinese Code [Ministry of Housing and Urban-Rural Development of the China (2015)]. Then, after integrating the acceleration twice, the displacement was obtained, as shown in Fig. 16. The propagation velocity was 1000 m/s. The static general analysis was adopted. The time step was 0.05 s, and the total time was 20 s. The computation time of each model was about 4 h. The largest maximal von-Mises stresses for the four sites of the two steel pipes are shown in Tab. 4.

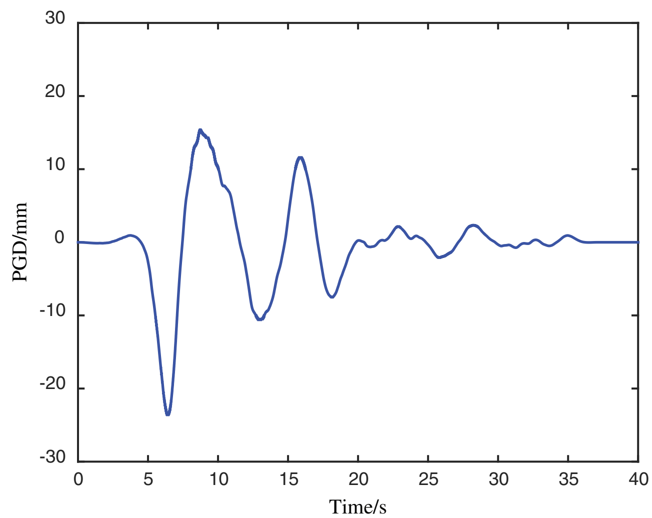

Figure 16: Displacement time history of the El Centro wave, 1979

Table 4: Largest maximal stress of the pipes in the utility tunnel for different sites

Diameter	Site I	Site II	Site III	Site IV
DN400	17.33 MPa	17.12 MPa	17.01 MPa	16.88 MPa
D159	6.52 MPa	6.44 MPa	6.39 MPa	6.34 MPa

For the above results, the pipe responses in the utility tunnel for the four sites showed few differences. For a DN400 pipe, the minimum of the largest maximal stress was 16.88 MPa at site IV, and the maximum was 17.33 MPa at site I. For a D159 pipe, the minimum of the largest maximal stress was 6.34 MPa at site IV, whereas the maximum was 6.52 MPa at site I. The maxima were only 2.8% higher than the minima. Thus, the influence of the sites was very small; i.e., the soil spring stiffness corresponding to different sites had small influence on the pipe seismic responses.

3.4 Influence of the wave propagation velocity

To study the influence of the wave propagation velocity, four propagation velocities were chosen, i.e., 300 m/s, 500 m/s, 1000 m/s, and 2000 m/s. Site II and the El Centro earthquake with a peak acceleration of 0.2 *g* were adopted. The largest maximal von-Mises stresses of the pipes are shown in Tab. 5.

Table 5: Largest maximal stresses of the pipes in the utility tunnel for different wave propagation velocities

Diameter	v_s**=300 m/s**	v_s**=500 m/s**	v_s**=1000 m/s**	v_s**=2000 m/s**
DN400	63.67 MPa	35.38 MPa	17.12 MPa	8.57 MPa
D159	22.39 MPa	13.05 MPa	6.44 MPa	3.16 MPa

Tab. 5 shows that the pipe stress decreased with the increase of the wave propagation velocity. For the DN400 pipes in a utility tunnel, the largest maximal stress decreased from 63.67 MPa to 8.57 MPa as v_s increased from 300 m/s to 2000 m/s. For the D159 pipe in a utility tunnel, the largest maximal stress decreased from 22.39 MPa to 3.16 MPa as v_s increased from 300 m/s to 2000 m/s.

For the pipes in the utility tunnel, due to the large rigidity of the utility tunnel and the constraint of the vertical movement of the pipe at the piers, it could be considered that the pipe at the piers moved together with the utility tunnel in the vertical direction. For the pipe near the joint of the utility tunnel, the vertical displacement of the two segments of the utility tunnel at the piers was different. The larger the difference, the greater the stress in the pipe. In order to explore the law of the pipe's stress, the vertical displacement difference of the two segments of the utility tunnel at the piers was deduced as shown below. This difference was called ΔS.

In Fig. 17, the x-axis is the axial direction of the pipe porch, and the y-axis is the direction of vertical displacement s. The angle between the propagation direction of the seismic wave and the x-axis is α. O and A represent the two piers, and the distance is L.

From the theory of an elastic wave, the field displacement s' in the propagation direction of the wave can be written as Eq. (13)

$$s' = f'(vt + x'), \tag{13}$$

where x' is the distance traveled by the ground motion in the propagation direction, v is the propagation velocity of the wave, t is the time parameter, and $f'(\cdot)$ is a displacement time history function.

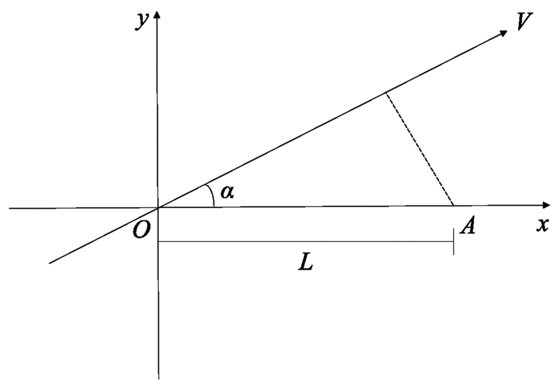

Figure 17: Schematic diagram of seismic propagation direction

In the y-axis direction, the field displacement s can be obtained as Eq. (14)

$$s = f'(vt + x \cdot \cos\alpha)\sin\alpha, \tag{14}$$

where x is the distance in the direction of the x-axis.

According to the common displacement method [Newmark (1967)], it was assumed that the vertical displacement S of the utility tunnel was equal to the site displacement s.

Therefore, the vertical displacement difference of the two segments of utility tunnel ΔS could be written as Eq. (15)

$$\Delta S = f'(vt + (x + L) \cdot \cos\alpha)\sin\alpha - f'(vt + x \cdot \cos\alpha)\sin\alpha. \tag{15}$$

If L is far less than the length of the utility tunnel, ΔS can be approximately written as Eq. (16)

$$\Delta S = \frac{\partial f'}{\partial x} \cdot \cos\alpha \cdot \sin\alpha \cdot L. \tag{16}$$

Assuming $vt + x'$ is u, f' is derived for x and t, respectively,

$$\frac{\partial f'}{\partial x} = \frac{\partial f'}{\partial u} \cdot \frac{\partial u}{\partial x} = \frac{\partial f'}{\partial x} \tag{17}$$

$$\frac{\partial f'}{\partial t} = \frac{\partial f'}{\partial u} \cdot \frac{\partial u}{\partial t} = v \cdot \frac{\partial f'}{\partial x} \tag{18}$$

In addition, the speed V of the site vibration can be expressed as follows:

$$V = \frac{\partial f'}{\partial t}. \tag{19}$$

According to Eqs. (17)-(19), $\dfrac{\partial f'}{\partial x}$ can be obtained as follows:

$$\frac{\partial f'}{\partial x} = \frac{V}{v}. \tag{20}$$

After Eq. (16) is considered, maximum of ΔS for the joint of the utility tunnel can be obtained as follows:

$$\Delta S = \frac{PGV}{v} \cdot \cos\alpha \cdot \sin\alpha \cdot L. \tag{21}$$

where PGV is peak velocity of the earthquake.

It is not difficult to see that the vertical displacement difference experienced by the pipe around the joint was proportional to the earthquake peak velocity value and inversely proportional to the earthquake wave propagation velocity. Correspondingly, the peak stress of the pipe, which was a linear function of the vertical displacement difference of the piers, was also subject to this law.

3.5 Influence of the seismic waves

Earthquakes are a complex stochastic process. For different earthquakes, the seismic responses of pipes may vary greatly. Eight actual earthquake records (Tab. 2) and two records corresponding to one site were used to study the influence of different seismic waves. The peak accelerations of all the seismic waves were adjusted to 0.2 *g*. The wave propagation velocity v_s was set to 1000 m/s. The largest maximal von-Mises stresses of the pipes are shown in Tab. 6.

Tab. 6 shows that although the peak accelerations of all the earthquake records were adjusted to 0.2 *g*, the largest maximal stresses of the pipes vary greatly. The largest maximal stresses under the El Centro Earthquake (1979) were larger than the other maximal stresses. Compared with the largest maximal stresses under the Mexico Earthquake, the former stress was 9.4 times larger for DN400, while it was 8.5 times larger for D159. Moreover, the largest maximal stresses had a positive correlation to the peak velocities of the seismic waves. The peak ground velocity of the El Centro earthquake (1979) was 5.1 times larger than that of the Mexico earthquake. For the other earthquakes, such as the Morgan Hill and Tangshan earthquakes, the largest maximal stresses were 0.37 and 0.58 times that of El Centro earthquake for DN400 pipes, and 0.36 and 0.50 times that of El Centro earthquake for D159 pipes. The peak ground velocities of the former two earthquakes were 0.44 and 0.62 times that of El Centro earthquake (1979). This positive correlation can be illustrated as shown in Eq. (12), which shows that a higher peak velocity resulted in higher largest maximal stresses. It should be noted that the process of deriving Eq. (12) ignored the pipe-soil interaction; i. e. the pipe and soil did not move together during earthquakes. Therefore, the maximal stress was not strictly proportional to maximal peak ground velocity.

Table 6: Largest maximal von-Mises stresses of the pipes for different earthquake records

Earthquake Records	Peak Velocity (mm/s)	Largest Maximal Stress in DN400 (MPa)	Largest Maximal Stress in D159 (MPa)
1985, La Union, Michoacan Mexico	66.53	1.83	0.76
1994, Los Angeles Griddith Observation	99.20	3.87	1.47
1952, Taft Lincoln school tunnel, California	150.36	6.35	2.33
1979, El-Centro, Array#10, Imperial valley	338.4	17.12	6.44
1984, Coyote Lake Dam, Morgan Hill	150.5	6.31	2.34
1940, El Centro-Imp Vall Irr Dist, El Centro	130.0	7.63	2.87
1976, Tianjin Hospital, Tangshan	208.6	9.87	3.23
1981, Westmorland, Westmorland	82.8	3.13	1.19

4 Comparison of the buried pipes and the pipes in the utility tunnel

4.1 Model of the buried pipes

Two buried pipes, which were the same as the pipes in the utility tunnel, were studied in order to compare their seismic performance. Similar to the utility tunnel, the elastic foundation beam method was adopted to simulate the buried pipes. Seventy-five groups of soil springs were distributed in the axial direction at a distance of 2 m. Each group consisted of four soil spring units uniformly arranged along the cross section of the pipe. The schematic of the model is shown in Fig. 18. The lengths of the buried pipes were 150 m, which was long enough to avoid the influence of boundary conditions. The soil spring stiffness of the two buried pipes obtained from the ALA-ASCE Guidelines [American Lifeline Alliance (2001, 2005)] are given in Tabs. 7 and 8. The buried pipes model is shown in Fig. 19. There were 14,464 nodes and 7200 elements in this model. The damping coefficient was 0 in this model.

4.2 Characteristics of the buried pipe in an earthquake

The seismic responses of the pipes in site II for the El Centro wave with a propagation velocity of 1000 m/s and a peak acceleration value of 0.2 *g* were studied. The static

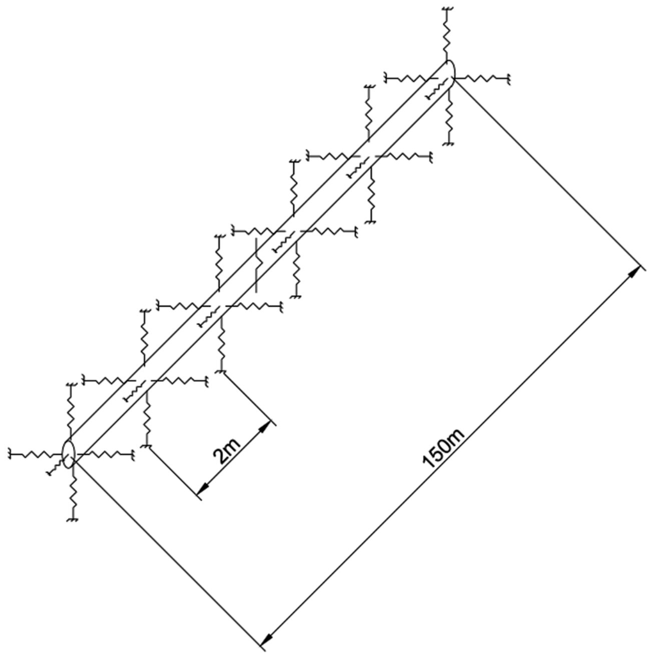

Figure 18: Schematic diagram of the utility tunnel model

Table 7: Soil spring stiffness of the DN400 pipe

Site	I	II	III	IV
Axial (kN/m^{-2})	9.51×10^6	1.10×10^7	1.02×10^7	5.77×10^6
Transverse (horizontal) (kN/m^{-2})	5.34×10^6	9.03×10^5	2.28×10^6	1.54×10^6
Transverse (vertical downwards) (kN/m^{-2})	3.24×10^6	7.67×10^5	3.83×10^5	1.91×10^5
Transverse (vertical upwards) (kN/m^{-2})	3.12×10^7	4.14×10^6	5.97×10^6	3.98×10^6

Table 8: Soil spring stiffness of D159 pipe

Site	I	II	III	IV
Axial (kN/m^{-2})	3.78×10^6	4.40×10^6	3.82×10^6	2.15×10^6
Transverse (horizontal) (kN/m^{-2})	3.50×10^6	7.46×10^5	9.55×10^5	6.46×10^5
Transverse (vertical downwards) (kN/m^{-2})	2.72×10^6	6.04×10^5	2.86×10^5	2.14×10^5
Transverse (vertical upwards) (kN/m^{-2})	1.80×10^7	4.01×10^6	5.99×10^6	4.50×10^6

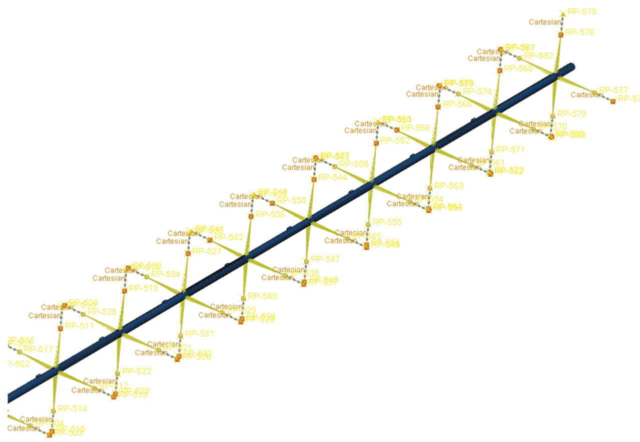

Figure 19: Buried pipes model

general analysis was adopted. The time step was 0.05 s, and the total time was 20 s. Fig. 20 shows the von-Mises stress contour of the middle part of the buried pipe (DN400) at 7.0 s for the El Centro (1979) wave. Fig. 21 shows the von-Mises contour of the middle part of the buried pipe (D159) at 7.0 s for the El Centro (1979) wave. Fig. 22 shows the Von-Mises stress envelope diagram of the buried pipes, wherein the distance refers to the distance from the end of the pipe where the seismic wave was input, along the direction of the pipe. It is clear that the maximal stress in the middle part of the pipe was in a stable stage.

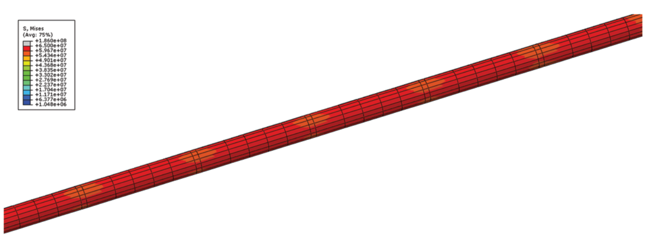

Figure 20: Von-Mises stress contour of buried pipes at 7.0 s (DN400)

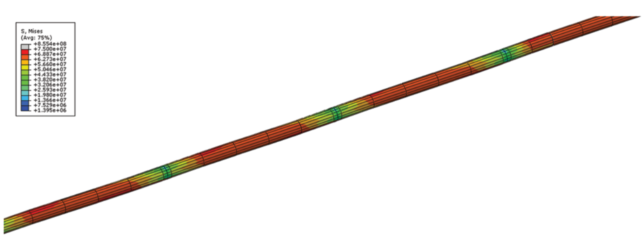

Figure 21: Von-Mises stress contour of buried pipes at 7.0 s (D159)

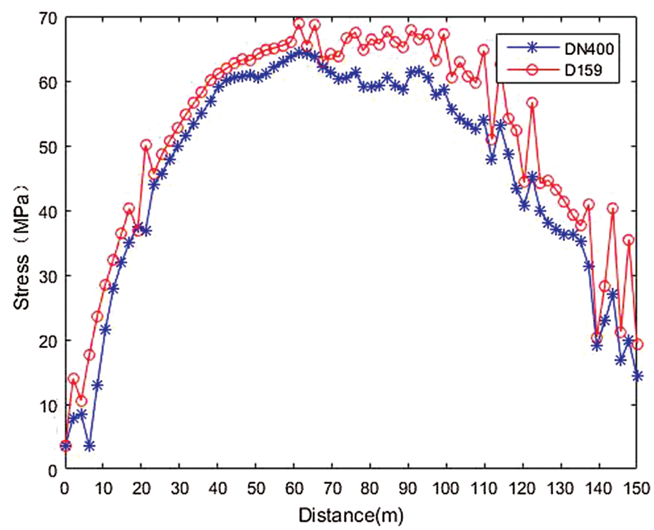

Figure 22: Von-Mises stress envelope diagram of buried pipes

4.3 Study of the parameters of buried pipes and comparison with the pipes in the utility tunnels

The influences of the site types, wave propagation velocities, and earthquake records on the seismic responses of buried pipes were also studied. The parameters were the same as those of the utility tunnel. The results are shown in Tabs. 9-11. It was not difficult to determine that the conclusions discussed in the previous Sections 3.3-3.5 were also reasonable for buried pipes.

Moreover, the seismic responses of the pipe in the utility tunnel and the buried pipes for eight earthquake records are shown in Tabs. 12 and 13.

For the two types of pipes, the maximal stresses of the pipes in the utility tunnel were much less than the corresponding stresses of the buried pipes. For example, when subjected to the

Table 9: Largest maximal stresses of buried pipes in different sites

Diameter	Site I	Site II	Site III	Site IV
DN400	64.68 MPa	64.21 MPa	63.71 MPa	63.07 MPa
D159	69.55 MPa	68.79 MPa	68.39 MPa	67.83 MPa

Table 10: Largest maximal stresses of buried pipes for different wave velocities

Diameter	v_s=300 m/s	v_s=500 m/s	v_s=1000 m/s	v_s=2000 m/s
DN400	200.30 MPa	123.13 MPa	64.21 MPa	31.38 MPa
D159	230.87 MPa	134.38 MPa	68.79 MPa	35.64 MPa

Table 11: Largest maximal stresses of buried pipes for different seismic waves

Earthquake Records	Earthquake Peak Velocity (mm/s)	Largest maximal Stress in DN400 (MPa)	Largest maximal Stress in D159 (MPa)
1985, La Union, Michoacan Mexico	66.53	11.29	12.93
1994, Los Angeles Griddith Observation	99.20	14.09	16.30
1952, Taft Lincoln school tunnel, California	150.36	25.58	28.71
1979, El-Centro, Array#10, Imperial valley	338.4	64.21	68.79
1984, Coyote Lake Dam, Morgan Hill	150.5	30.22	34.95
1940, El Centro-Imp Vall Irr Dist, El Centro	130.0	33.57	38.59
1976, Tianjin Hospital, Tangshan	208.6	38.59	44.02
1981, Westmorland, Westmorland	82.8	15.12	17.29

El Centro earthquake (1979) and the Tangshan earthquake (1976), the maximal stresses of the DN400 pipes in the utility tunnel were 17.12 MPa and 9.87 MPa, respectively, whereas the stresses of the corresponding buried pipes were 64.21 MPa and 38.59 MPa.

In addition, for the buried pipes, the stresses of the pipes with large diameters were lower because the seismic wave acted on the pipe through the soil spring. For large-diameter pipes, the pipe stiffness was larger, and thus, the soil spring was relatively softer and absorbed more strain. Correspondingly, the seismic response of the buried pipe with a large diameter was lower. However, for pipes in the utility tunnel, the stress of the pipe with a large diameter was larger because the axial stresses of different pipes in the utility tunnel could be neglected. However, the bending stress of the pipe with a large diameter was larger than that of the pipe with a small diameter. Taking the results under El Centro (1979) seismic wave as an example, the maximum bending stresses of the D159 and DN400 pipes were 17.12 MPa and 6.44 MPa, respectively. Apparently, the bending stress of DN 400 pipe was about 2.6 times that of the D159 pipe. Thus, the stress of the DN400 pipe was larger than that of the D159 pipe.

Table 12: Seismic response of the pipe in utility tunnel and the buried pipes (DN400)

Seismic Wave	Maximal stress in pipe around joint 1 (MPa)	Maximal stress in pipe around joint 2 (MPa)	Maximal stress in middle pipe around pier (MPa)	Maximal stress in suspended middle pipe (MPa)	Largest maximal stress in buried pipe (MPa)
1985, La Union, Michoacan Mexico	1.83	1.80	0.45	0.17	11.29
1994, Los Angeles Griddith Observation	3.87	3.76	1.14	0.21	14.09
1952, Taft Lincoln school tunnel, California	6.32	6.35	1.73	0.21	25.58
1979, El-Centro, Array#10, Imperial valley	17.12	16.97	5.37	0.82	64.21
1940, El Centro-Imp Vall Irr Dist, El Centro	7.54	7.63	2.35	0.33	30.22
1984, Coyote Lake Dam, Morgan Hill	6.31	6.21	1.31	0.32	33.57
1976, Tianjin Hospital, Tangshan	9.87	9.82	1.89	0.45	38.59
1981, Westmorland, Westmorland	3.13	3.11	0.84	0.19	15.12

Table 13: Seismic response of the pipe in a utility tunnel and the buried pipe (D159)

Seismic Wave	Maximal stress in pipe around joint 1 (MPa)	Maximal stress in pipe around joint 2 (MPa)	Maximal stress in middle pipe around pier (MPa)	Maximal stress in middle pipe suspended (MPa)	Largest maximal stress in buried pipe (MPa)
1985, La Union, Michoacan Mexico	0.76	0.73	0.22	0.13	12.93
1994, Los Angeles Griddith Observation	1.47	1.45	0.42	0.23	16.30
1952, Taft Lincoln school tunnel, California	2.27	2.33	0.28	0.17	28.71
1979, El-Centro, Array#10, Imperial valley	6.44	6.40	2.10	0.37	68.79
1940, El Centro-Imp Vall Irr Dist, El Centro	2.87	2.81	0.87	0.23	34.95
1984, Coyote Lake Dam, Morgan Hill	2.34	2.50	0.81	0.27	38.59
1976, Tianjin Hospital, Tangshan	3.23	3.17	1.53	0.36	44.02
1981, Westmorland, Westmorland	1.19	1.17	0.35	0.16	17.29

5 Conclusion

To study pipes in utility tunnels, utility tunnels were modeled with the elastic foundation beam method considering the traveling wave effect. The seismic responses of the pipes in the utility tunnels were obtained, and the effects of the site type, wave propagation velocity, and different earthquake records were analyzed. Models of buried pipes were also established for comparison. The following conclusions were derived from the results.

1. High stresses appeared for pipes in a utility tunnel, at locations close to the joints between two utility tunnel segments.
2. The soil spring stiffness seemed to have almost no influence on the seismic response of the structures. A reasonable result could be obtained only if the soil spring coefficient was generally within an appropriate range.
3. For different engineering fields, a positive correlation was found between the apparent velocity of the site and seismic responses of the pipes.
4. For underground structures, the maximal earthquake response depended more on the peak velocity of the seismic wave.
5. Utility tunnels helped to greatly reduce the maximum stress on pipes since the axial deformation at the pipe ends was not restrained.

Funding Statement: This research is supported by the Ministry of Science and Technology of China (SLDRCE19-B-24). Wei Liu is the author who received the grant. The URLs to sponsors' website is http://www.most.gov.cn/.

Conflicts of Interest: The authors declare that they have no conflicts of interest to report regarding the present study.

References

American Lifeline Alliance. (2001): *Guidelines for Design of Buried Steel Pipes*. ASCE Press, Washington.

American Lifeline Alliance. (2005): *Seismic Guidelines for Water Pipe*. Washington: FEMA Press.

Bao, X.; Xia, Z.; Ye, G.; Fu, Y.; Su, D. (2017): Numerical analysis on the seismic behavior of a large metro subway tunnel in liquefiable ground. *Tunnelling and Underground Space Technology*, vol. 66, pp. 91-106. DOI 10.1016/j.tust.2017.04.005.

Bettess, P.; Zienkiewica, O. C. (1977): Diffraction and refraction of surface wave using finite and infinite elements. *International Journal for Numerical Methods in Engineering*, vol. 11, no. 8, pp. 1271-1290. DOI 10.1002/nme.1620110808.

Cao, Z.; Zhou, Y.; Xu, P.; Li, J. (2014): Mechanical response analysis and safety assessment of shallow-buried pipeline under the influence of mining. *Computer Modeling in Engineering & Sciences*, vol. 101, no. 5, pp. 351-364.

Chao, C. (1973): *Diffraction of Elastic Waves and Dynamic Stress Concentrations*. New York: Crane, Russak.

Chen, J.; Shi, X. J.; Li, J. (2010): Shaking table test of utility tunnel under non-uniform earthquake wave excitation. *Soil Dynamics and Earthquake Engineering*, vol. 30, no. 11, pp. 1400-1416. DOI 10.1016/j.soildyn.2010.06.014.

Hu, Y.; Fang, H.; Wang, F.; Zhai, K. (2019): Full-scale test and numerical simulation study on load-carrying capacity of prestressed concrete cylinder pipe (PCCP) with broken wires under internal water pressure. *Engineering Failure Analysis*, vol. 104, pp. 513-530. DOI 10.1016/j.engfailanal.2019.06.049.

Jiang, L. Z.; Chen, J.; Li, J. (2009). Dynamic response analysis of underground utility tunnel during the propagation of Rayleigh waves. *International Conference on Pipeline and Trenchless Technology. China*. pp. 1174-1182. 10.1061/9780784410738.

Kuesel, T. R. (1969): Earthquake design criteria for subway. *Journal of the Structural Division*, vol. 95, pp. 1213-1231.

Kuribayashi, E.; Iwasaki, T.; Kawashima, K. (1974): Dynamic behavior of a subsurface tubular structure. *Proceedings of 5th European Conference on Earthquake Engineering*, vol. 7, no. 4, pp. 200-209.

Kuwata, Y.; Takada, S.; Yamasaki, S. (2008). Seismic performance of complicated pipe network. *Proceedings of 14th World Conference on Earthquake Engineering*. *Beijing*. pp. 12-17.

Lai, J.; He, S.; Qiu, J.; Chen, J.; Wang, L. et al. (2017): Characteristics of seismic disasters and aseismic measures of tunnels in Wenchuan earthquake. *Environmental Earth Sciences*, vol. 76, no. 2, pp. 103. DOI 10.1007/s12665-017-6405-3.

Lee, V. W. (1979): Response of tunnels to incident SH waves. *Journal of Engineering Mechanics*, vol. 105, no. 4, pp. 643-659.

Li, J. (1999): Behavior control and earthquake response analysis of complex lifeline systems. *Bulletin of National Natural Science Foundation of China* (in Chinese), vol. 6, pp. 17-20.

Li, B.; Fang, Y.; He, W.; Sun, B. (2017): Stability analysis of cross-channel excavation for existing anchor removal project in subway construction. *Computer Modeling in Engineering & Sciences*, vol. 113, no. 1, pp. 57-69.

Li, B.; Fang, H.; He, H.; Yang, K.; Chen, C. et al. (2019): Numerical simulation and full-scale test on dynamic response of corroded concrete pipelines under multi-field coupling. *Construction and Building Materials*, vol. 200, pp. 368-386. DOI 10.1016/j.conbuildmat.2018.12.111.

Liao, Z. P. (2002): *Introduction to Wave Motion Theories in Engineering*. Beijing: Science Press.

Liu, W.; Li, J. (2008): Stochastic seismic response of pipelines with corrosion. *Journal of Earthquake Engineering*, vol. 12, no. 6, pp. 914-931. DOI 10.1080/13632460801890190.

Liu, W.; Sun, Q.; Miao, H.; Li, J. (2015): Nonlinear stochastic seismic analysis of buried pipe systems. *Soil Dynamics and Earthquake Engineering*, vol. 74, pp. 69-78. DOI 10.1016/j.soildyn.2015.03.017.

Luco, J. E.; de Barros, F. C. P. (1994): Dynamic displacements and stresses in the vicinity of a cylindrical cavity embedded in a half-space. *Earthquake Engineering & Structural Dynamics*, vol. 23, no. 3, pp. 321-340. DOI 10.1002/eqe.4290230307.

Mandolini, A.; Minutolo, V.; Ruocco, E. (2001): Coupling of underground pipelines and slowly moving landslides by BEM analysis. *Computer Modeling in Engineering & Sciences*, vol. 2, no. 1, pp. 39-48.

Ministry of Housing and Urban-Rural Development of the China (2015): *GB50011-2015: Code for Seismic Design of Buildings*. Beijing: China Architecture & Building Press.

Newmark, N. M. (1967). Problems in wave propagation in soil and rock. *Proceedings International Symposium on Wave Propagation and Dynamic Properties of Earth Materials*. *Albuquerque*, pp. 7-26.

O'Rourke, M.; Liu, X. (1999): *Response of Buried Pipes Subject to Earthquake Effects*. Baffalo, NY: MCEE.

Pao, Y. H. (1962): Dynamical stress concentration in an elastic plate. *Journal of Applied Mechanics*, vol. 29, no. 2, pp. 299-305. DOI 10.1115/1.3640545.

Parmelee, R.; Ludtke, C. (1975). Seismic soil-interaction of buried pipes. *Proceedings of US. National Conference on Earthquake Engineering*. *Ann Arbor, MI*. pp. 406-415.

Qu, T. J.; Wang, Q. X. (1993): Series solutions for the axial vibration of buried pipeline under earthquake excitation. *Earthquake Engineering and Engineering Vibration* (in Chinese), vol. 13, no. 4, pp. 39-45.

Sei, ASCE (2010): *Minimum Design Loads for Buildings and Other Structures: ASCE Standards ASCE/SEI 7-10*. ASCE.

Shinozuka, M.; Koike, T. (1979): Estimation of structural strains in underground lifeline pipes. *International Journal of Pressure Vessels and Piping*, vol. 34, pp. 31-48.

Song, C. M.; Wolf, J. P. (1994): Dynamic stiffness of unbounded medium based on damping-solvent extraction. *Earthquake Engineering & Structural Dynamics*, vol. 23, no. 2, pp. 169-181. DOI 10.1002/eqe.4290230205.

Song, C. M.; Wolf, J. P. (2000): The scaled boundary finite element method-a primer solution procedures. *Computers and Structures*, vol. 78, no. 3, pp. 211-225. DOI 10.1016/S0045-7949 (00)00100-0.

St John, C. M.; Zahrah, T. F. (1987): Aseismic design of underground structures. *Tunneling and Underground Space Technology*, vol. 2, no. 2, pp. 165-197. DOI 10.1016/ 0886-7798(87)90011-3.

State Key Laboratory of Disaster Reduction in Civil Engineering (2008): *Earthquake Damage in Wenchuan Earthquake* (in Chinese). Shanghai: Tongji University Press.

Su, D.; Kang, Y.; Wang, X.; Zheng, A.; Li, D. et al. (2016): Analysis and numerical simulation for tunnelling through coal seam assisted by water jet. *Computer Modeling in Engineering & Sciences*, vol. 111, no. 5, pp. 375-393.

Sun, Q. W. (2012), *Seismic Response Analysis Model and Reliability Analysis of Buried Water Supply Systems (in Chinese) (Ph.D. Thesis)*. Tongji University, China.

Tang, A. P.; Gai, Z. B.; Wen, A. H.; You, H. Y. (2012). Seismic isolation simulation of pipe in utility tunnel. *International Conference on Pipeline and Trenchless Technology. China*. pp. 1534-1541.

Wang, L. R. L.; Cheng, K. M. (1979): Seismic response behavior of buried pipe. *Journal of Pressure Vessel Technology*, vol. 101, no. 1, pp. 21-30. DOI 10.1115/1.3454594.

Wang, J. X.; Guo, E. D.; Zhang, M. J. (2012): Analysis and countermeasures on seismic damages to gas pipe in Wenchuan earthquake. *World Earthquake Engineering* (in Chinese), vol. 4, pp. 44-50.

Wu, L.; Xiang, X.; Chen, Y.; Ali, K.; Zhou, J. et al. (2019): Modeling and simulation of dynamic unloading of prestressed rockmass. *Computer Modeling in Engineering & Sciences*, vol. 120, no. 2, pp. 421-443. DOI 10.32604/cmes.2019.05218.

Xu, H.; Li, T.; Xia, L.; Zhao, J. X.; Wang, D. (2016): Shaking table tests on seismic measures of a model mountain tunnel. *Tunnelling and Underground Space Technology*, vol. 60, pp. 197-209. DOI 10.1016/j.tust.2016.09.004.

Yu, H. T.; Yan, X.; Bobet, A.; Yuan, Y.; Xu, G. et al. (2017): Multi-point shaking table test of a long tunnel subjected to non-uniform seismic loadings. *Bulletin of Earthquake Engineering*, vol. 16, no. 2, pp. 1041-1059. DOI 10.1007/s10518-017-0223-6.

Yu, H. T.; Yuan, Y.; Xu, G.; Su, Q.; Yan, X. et al. (2018a): Multi-point shaking table test for long tunnels subjected to non-uniform seismic loadings - part II: application to the HZM immersed tunnel. *Soil Dynamics and Earthquake Engineering*, vol. 108, pp. 187-195.

Yu, H. T.; Zhang, Z. W.; Chen, J. T.; Bobet, A.; Zhao, M. et al. (2018b): Analytical solution for longitudinal seismic response of tunnel liners with sharp stiffness transition. *Tunnelling and Underground Space Technology*, vol. 77, pp. 103-114.

Yue, Q. X. (2007): *Seismic Response Analysis and Reliability of Utility Tunnel (in Chinese) (Ph.D. Thesis)*. Tongji University, China.

Zhao, Z.; Song, E. X. (2015): Particle mechanics modeling of creep behavior of rockfill materials under dry and wet conditions. *Computers and Geotechnics*, vol. 68, pp. 137-146. DOI 10.1016/j.compgeo.2015.04.008.